PHYSICAL REVIEW B **86**, 134425 (2012)

Possible skyrmion-lattice ground state in the *B*20 chiral-lattice magnet MnGe as seen via small-angle neutron scattering

N. Kanazawa,[1] J.-H. Kim,[2] D. S. Inosov,[2] J. S. White,[3,4] N. Egetenmeyer,[3] J. L. Gavilano,[3]
S. Ishiwata,[1] Y. Onose,[5] T. Arima,[6,7] B. Keimer,[2] and Y. Tokura[1,8]

[1]*Department of Applied Physics and Quantum Phase Electronics Center (QPEC), University of Tokyo, Tokyo 113-8656, Japan*
[2]*Max Planck Institute for Solid State Research, Heisenbergstraße 1, 70569 Stuttgart, Germany*
[3]*Laboratory for Neutron Scattering, Paul Scherrer Institut, CH-5232 Villigen, Switzerland*
[4]*Laboratory for Quantum Magnetism, Ecole Polytechnique Fédérale de Lausanne, CH-1015 Lausanne, Switzerland*
[5]*Department of Basic Science, University of Tokyo, Tokyo 153-8902, Japan*
[6]*Department of Advanced Materials Science, University of Tokyo, Kashiwa 277-8561, Japan*
[7]*RIKEN SPring-8 Center, Sayo, Hyogo 679-5148, Japan*
[8]*Cross-Correlated Materials Research Group (CMRG) and Correlated Electron Research Group (CERG), RIKEN Advanced Science Institute, Wako 351-0198, Japan*

(Received 2 September 2012; revised manuscript received 4 October 2012; published 25 October 2012)

We have investigated the magnetic structure in a polycrystalline sample of the *B*20-type MnGe by means of small-angle neutron scattering. On the projected diffraction plane normal to the incoming neutron beam, a Debye-ring-like pattern appears due to the random orientation of the spin helix q vectors ($\parallel \langle 100 \rangle$). When an external magnetic field is applied normal to the incoming neutron beam, an intense peak with wave vector (q) perpendicular to the applied magnetic field is observed as the hallmark of the formation of a skyrmion lattice with a multiple-q helix in a wide temperature-magnetic-field region. This scattering intensity remains even after removing the magnetic field, which indicates that a skyrmion lattice is stabilized as the ground state. A different form of skyrmion lattice, either square or cubic, is proposed, which is also shown to be in good agreement with previous high-angle neutron diffraction results. Calculations based on such structures also describe the magnetic-field profile of the topological Hall resistivity.

DOI: 10.1103/PhysRevB.86.134425 PACS number(s): 75.25.−j, 75.70.Kw, 72.15.Gd

I. INTRODUCTION

The antisymmetric spin exchange interaction affected by the relativistic effect, termed the Dzyaloshinskii-Moriya (DM) interaction,[1,2] plays a role in twisting spin order, and hence gives rise to various kinds of non-collinear and non-coplanar magnetic structures. Weak ferromagnetism in α-Fe_2O_3 (Refs. 1 and 2) and the helical spin order in MnSi (Ref. 3) are typical examples found in the early stage of research. In recent years, some other magnetic structures have been experimentally observed in FeSi-type (*B*20-type) chiral-lattice magnets: partial order in the high-pressure phase of MnSi,[4] a magnetic blue phase,[5,6] a Swiss-roll-like helical structure in FeGe,[7] and a triangular lattice of skyrmions in some compounds (MnSi,[8] $Fe_{1-x}Co_xSi$,[9,10] FeGe,[11–13] etc.[14]). Among them, the magnetic skyrmion lattice is attracting much attention and is providing an excellent laboratory for novel emergent electromagnetic responses[15] (such as the topological Hall effect[16–18] and a skyrmion-motion-induced electric field[19–21]), which may have the potential for next-generation spintronic devices.[22–24] Since the initial prediction of skyrmion formation,[25] different types of skyrmion lattices have been proposed theoretically for DM magnets.[26–29,31] Such diversity of topological magnetic textures and emergent physical phenomena is the reason for the extensive research activities on *B*20-type chiral magnets.

The crystal structure of *B*20-type transition-metal compounds belongs to the space group $P2_13$, which lacks space inversion symmetry and hosts DM interactions [Fig. 1(a)]. The following generic magnetic phase diagram is observed in *B*20-type compounds:[14] A long-period (10–200 nm) helical (proper screw) spin structure whose helical plane is perpendicular to the wave vector is stabilized by the competition between ferromagnetic and DM interactions in zero magnetic field. Relatively weak magnetic anisotropy due to spin-orbit interaction locks the modulation vector q along $\langle 111 \rangle$ or $\langle 100 \rangle$. A certain magnetic field unpins and aligns the helical order along its direction, distorting the helical plane like an umbrella. This state is called conical spin structure. The transition to the induced ferromagnetic state occurs upon further increasing of the magnetic field. In addition, a triangular lattice of skyrmions, whose modulation directions are perpendicular to the magnetic field, is observed within a narrow temperature–magnetic-field window just below T_N at intermediate fields.[8,9,13,14,32] This skyrmion phase was once known as the A phase, in which not only anomalies in physical properties such as ultrasonic absorption,[33] electron spin resonance,[34] and magnetoresistance[35] but also q-flop perpendicular to the field[36,37] were already observed.

The topological Hall effect, which originates from the Berry phase gained by conduction electrons moving on a non-coplanar spin texture, is also one of the hallmarks of skyrmion-lattice systems. The topological Hall resistivity ρ_{yx}^T is detected in *B*20-type MnGe (Ref. 18) in analogy with other *B*20-type compounds.[16,38] However, not only the magnitude but also the field dependence of the topological Hall effect is very distinct from other compounds; ρ_{yx}^T begins to appear immediately upon the application of the magnetic field and persists up to the critical field H_c above which spins are fully aligned. Furthermore, the temperature region with discernible ρ_{yx}^T is very wide from 2 to 70 K. These observations indicate that skyrmions can exist as the ground state at zero magnetic

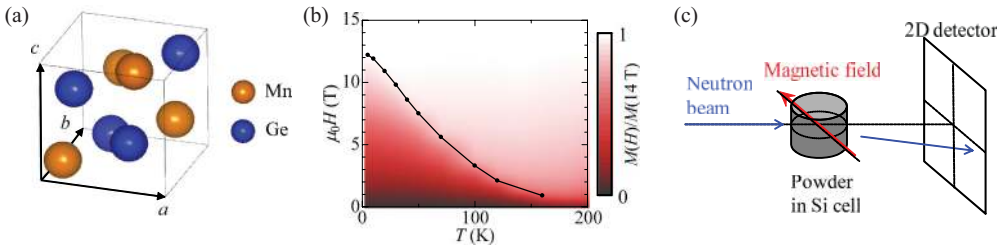

FIG. 1. (Color online) (a) Crystal structure of $B20$-type MnGe. (b) A contour map of magnetization normalized by its value at 14 T at every temperature. The black circles indicate the temperature variation of the critical field, at which the spin-collinear (ferromagnetic) state is realized. (c) SANS setup used in the present study. The powdered MnGe sample is put into a single-crystalline silicon cell. The magnetic field is applied perpendicular to the incident neutron beam.

field and are stable in a wide temperature (T)–magnetic-field (H) region in contrast to the confined T-H phase of the A phase in conventional $B20$-type compounds. [See also the phase diagram of MnGe in Fig. 1(b).] Indeed, various skyrmion ground states other than the triangular lattice form have been theoretically proposed,[26,27,29,31] and MnGe may be a candidate for those. In the following, we present results of small-angle neutron scattering (SANS) experiments on $B20$-type MnGe, which demonstrate the formation of a skyrmion lattice at zero magnetic field as well as in a wide T-H region, as expected. In addition, we discuss its possible lattice structure by analyzing the reported ρ_{yx}^{T} data[18] according to the theoretical formula proposed by Binz and Vishwanath.[30] Either a square or a simple-cubic skyrmion lattice is proposed here to be realized in MnGe.

II. EXPERIMENTS

The MnGe polycrystals were synthesized by the high-pressure method, as described in detail in Ref. 18. The SANS experiments were carried out using SANS-I instrument at the Paul Scherrer Institut using neutrons with wavelength 4.7 Å. A powder sample was packed in a single-crystalline silicon container with a height of 9.5 mm and a diameter of 18 mm, and installed in a cryomagnet. The magnetic field was applied perpendicular to the incident neutron beam collimated over 4.5 m. The diffracted neutrons were collected by a two-dimensional multidetector placed 2 m behind the sample [see Fig. 1(c)].

III. RESULTS AND DISCUSSIONS

A. SANS results

The SANS patterns during zero field cooling (ZFC) from room temperature are shown in Figs. 2(a)–2(f). A diffusive scattering intensity around $q = 0$ gradually grows with decreasing temperature above $T_N \approx 170$ K, and Debye-ring-like patterns are clearly observed below T_N, as evidenced by the angle-averaged diffracted intensity as a function of wave vector in Fig. 2(g). The enhancement of the intensity around $q = 0$ indicates that the magnetic correlation is developing well above T_N. On the other hand, the ring patterns below T_N are associated with the formation of a periodically modulated magnetic structure, and the radius of the diffracted neutron pattern, i.e., the magnitude of the magnetic modulation vector, increases with decreasing temperature from 1.15 nm^{-1} (151 K) to 2.23 nm^{-1} (30 K), which is in accord with previous reports [Fig. 2(h)].[18,39]

Figure 3 shows the development of SANS patterns under different magnetic fields at 30 K after ZFC. We could not access the gray-shaded region in Fig. 3 due to the angular limitation of the cryomagnet window. When applying a field of 2 T, three characteristic diffraction patterns appear: crescent-shaped intensity patterns parallel to the field $I(\boldsymbol{q} \parallel \boldsymbol{H})$ [patterns 1 and 2 in Fig. 3(b)], a local maximal intensity pattern perpendicular to the field $I(\boldsymbol{q} \perp \boldsymbol{H})$ [intensity 3 in Fig. 3(b)], and a diffusive pattern around the center $I_{\rm diff}$ [intensity 4 in Fig. 3(b)]. At higher magnetic fields of 4 and 6 T [Figs. 3(c) and 3(d)], $I(\boldsymbol{q} \perp \boldsymbol{H})$ almost disappears and the crescent shape of $I(\boldsymbol{q} \parallel \boldsymbol{H})$ shrinks. Around the critical field H_c (≈ 9.8 T at 30 K), all the intensities sharply drop [Fig. 3(e)]. When ramping the field down back to zero, the various overall SANS profiles at each magnetic field [Figs. 3(f) and 3(g)] are similar to those which were measured on increasing the field [Figs. 3(b) and 3(c)], although the ring pattern is not restored and all the characteristic intensities remain at zero magnetic field [Fig. 3(h)]. Rough alignment of the modulation directions parallel to the field is reflected by the crescent shape of $I(\boldsymbol{q} \parallel \boldsymbol{H})$, which is also detected in a single crystalline $B20$-type $Fe_{0.7}Co_{0.3}Si$ (Ref. 37). The shrinkage of the crescent shape indicates the gradual alignment of modulation vectors toward $\boldsymbol{q} \parallel \boldsymbol{H}$. $I_{\rm diff}$ (intensity 4) is assigned to the double scattering of the helical magnetic structure, representing the superposition of two crescent shapes of intensities 1 and 2. The emergence of intensity perpendicular to the applied field is a typical signature of the formation of a skyrmion lattice, which has been confirmed for the skyrmion-lattice state in other $B20$-type compounds.[8,36,37] We have also observed a ring pattern corresponding to $I(\boldsymbol{q} \perp \boldsymbol{H})$ in the setup with the magnetic field applied along the incident beam, which confirms the formation of a skyrmion lattice (not shown).

Here we should note that the magnetic field causes partial alignment of the MnGe powder grains as well. Once a magnetic field is applied to the sample, the ring-shaped SANS pattern below T_N gives way to an anisotropic crescent-shaped one, as shown in Fig. 3(h). The identical change happens even after initializing (randomizing) the magnetic state by increasing the sample temperature well above T_N (e.g., 300 K, not shown). This demonstrates that the easy axes of magnetization, which are ⟨100⟩ in MnGe,[18] are flipped along the field direction. Therefore, the peak intensities are observed again along the previous field direction, originating from the ⟨100⟩-modulated

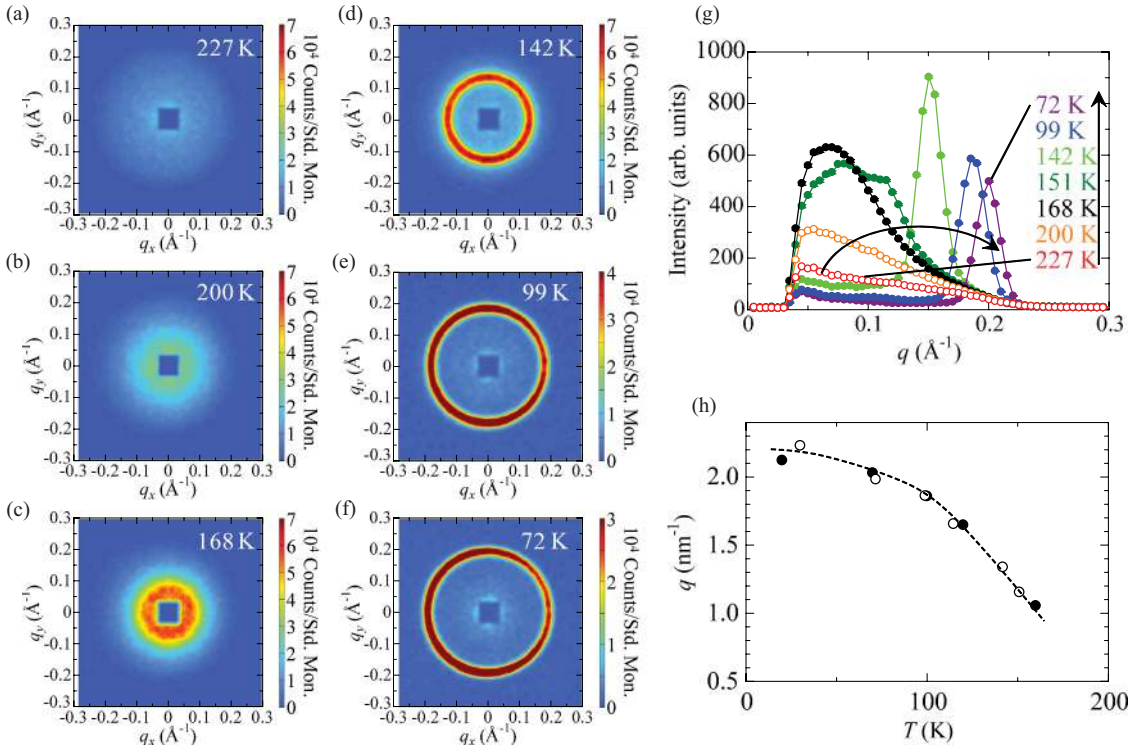

FIG. 2. (Color online) (a)–(f) SANS patterns at zero magnetic field during zero-magnetic-field cooling (ZFC). (g) The angle-averaged SANS intensity during ZFC as a function of wave vector q. (h) Temperature dependence of the magnetic modulation vector q (open circles) as measured in the present SANS study, compared with the data from the high-angle neutron diffraction study taken from Ref. 18 (solid circles).

magnetic structure at zero field. Although the polycrystalline powder is subjected to the magnetic-field induced alignment, the assignment of the $I(\boldsymbol{q} \perp \boldsymbol{H})$ diffraction to the formation of a skyrmion lattice is supported by the following arguments: (i) If MnGe were in a single-q screw or conical state, the magnetic field would not be able to rotate the modulation directions perpendicular to its direction. (ii) Furthermore, although we cannot determine whether a single-q or the multiple-q state (skyrmion lattice) produces the intensity $I(\boldsymbol{q} \perp \boldsymbol{H})$ because of using the polycrystalline sample, the multiple-q state with the non-coplanar spin configuration is a more plausible structure due to the existence of the topological Hall effect (*vide infra*). (iii) The hysteresis behavior of the H dependence of the magnetization in MnGe indicates that the modulation direction remains along the previously applied magnetic field once the field is increased above a critical value.[18] This feature is generically observed in other $B20$-type helimagnets, which is also confirmed by SANS experiments.[36,37] Therefore, the reappearance of $I(\boldsymbol{q} \perp \boldsymbol{H})$ with decreasing field [Figs. 3(g) and 3(h)] could hardly be explained without assuming the formation of the skyrmion-lattice state, which has q vectors perpendicular to the magnetic field.

To summarize the above, a magnetic structure modulated in multiple directions, most probably a skyrmion-lattice state, is stabilized as the ground state at zero magnetic field. Prior to the magnetic-field-induced orientation of the polycrystalline powder, the randomly oriented multiple-q structures produce the ring scattering pattern at zero magnetic field [Fig. 3(a)]. The magnetic field (H) flips and aligns the modulation directions as well as the crystalline grains with the ⟨100⟩ axes parallel to H, giving rise to accumulated intensities parallel to the field. In the multiple-q state, the other modulation directions are perpendicular to the field, which can show up as $I(\boldsymbol{q} \perp \boldsymbol{H})$. The multiple q vectors aligned by the magnetic field persist and point along the same directions after removing the field, which results in a SANS pattern at zero field [Fig. 3(h)] similar to the one under a magnetic field [Fig. 3(g)]. From the results of a high-angle neutron diffraction experiment,[18] it is clear that all the multiple modulation directions should belong to the category ⟨100⟩, i.e., [100] and equivalent, directions. Therefore, the ground state will be the multiple-q state composed of two or three independent ⟨100⟩ directions, which we define as a square or a simple-cubic (SC) skyrmion lattice, respectively. If the square skyrmion lattice is the case, the observed much larger intensity $I(\boldsymbol{q} \parallel \boldsymbol{H})$ than $I(\boldsymbol{q} \perp \boldsymbol{H})$ may indicate that the skyrmion lattice coexists with the helical structure producing $I(\boldsymbol{q} \parallel \boldsymbol{H})$. On the other hand, in the case of the simple-cubic lattice, one modulation vector gets collected along the magnetic field, and the set of the other two modulations can point to an arbitrary direction in the plane normal to the field, which may explain $I(\boldsymbol{q} \parallel \boldsymbol{H}) \gg I(\boldsymbol{q} \perp \boldsymbol{H})$.

Although some form of skyrmion lattice is likely to form in MnGe judging from the circumstantial evidences, i.e., the topological Hall effect and the appearance of $I(\boldsymbol{q} \perp \boldsymbol{H})$, there would be alternative scenarios to explain $I(\boldsymbol{q} \perp \boldsymbol{H})$ that involves only helices. For example, the grains may have cleavage surfaces of (100) and/or (110) planes,[40] whose normal vectors are perpendicular to the ⟨100⟩ direction aligned along the field direction. If the Hamiltonian includes a term that aligns the helical plane with the surface of the powder

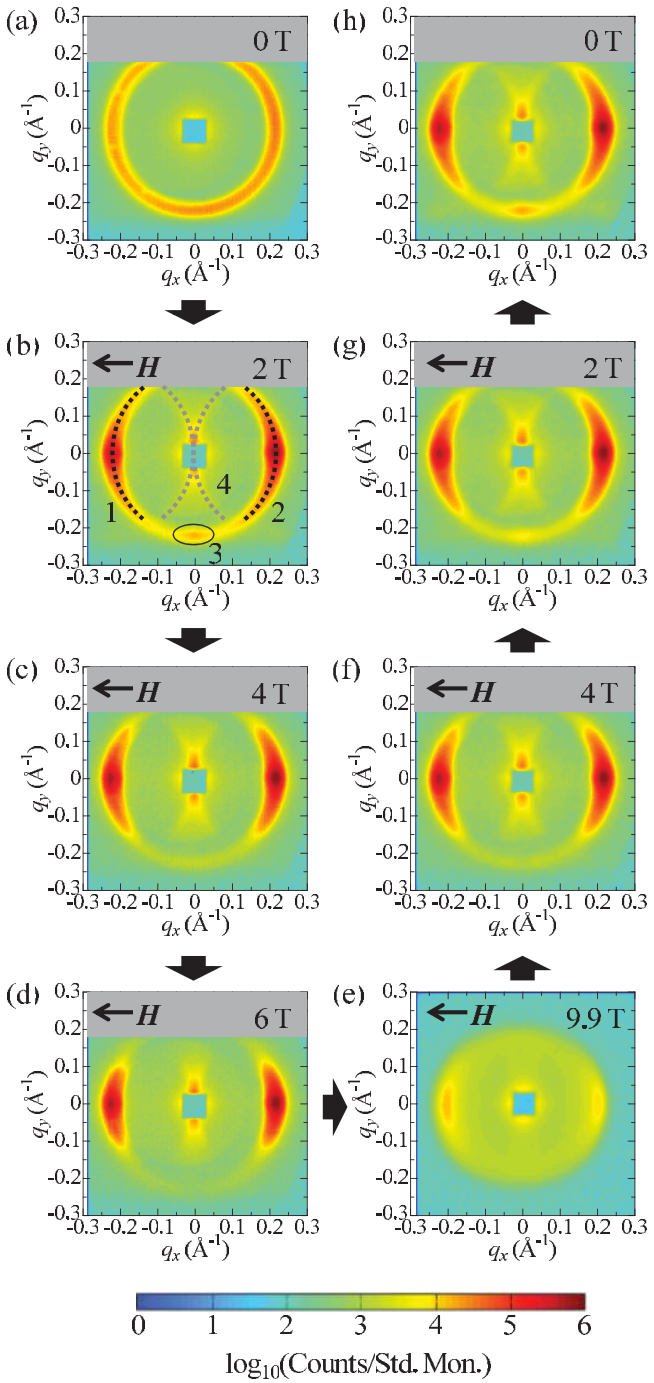

FIG. 3. (Color online) Variation of SANS patterns with magnetic field (H) at 30 K. The magnitude of the applied magnetic field changes from (a) 0 T to (e) 9.9 T and back to (h) 0 T in the sequential order indicated by thick arrows. Three typical intensities are clearly observed in panel (b): (i) crescent-shaped diffractions parallel to the field (diffractions 1 and 2); (ii) a local maximal intensity observed perpendicular to the field (diffraction 3), which indicates the formation of a skyrmion lattice; (iii) a diffusive diffraction around the center (diffraction 4), which is assigned to the double scattering stemming from the crescent shape of diffractions 1 and 2. The solid and dashed lines in panel (b) are guides to the eyes.

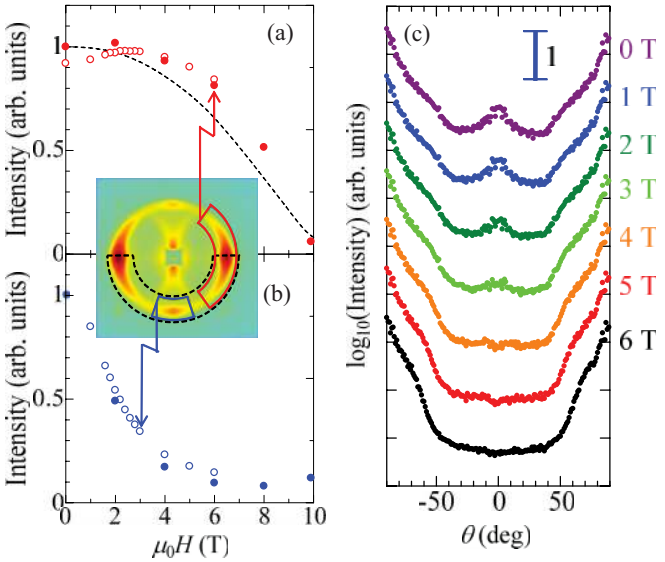

FIG. 4. (Color online) Magnetic-field dependence of SANS intensities (a) parallel and (b) perpendicular to the field at 30 K. Solid and open circles represent different field-decreasing scans. The dashed line in panel (a) indicates the relation $M_s^2 - M^2$ vs H. (c) SANS intensity as a function of angle in the sector bounded by the dashed line in the inset of panels (a) and (b). The angle origin ($\theta = 0$) is defined at the $I(\boldsymbol{q} \perp \boldsymbol{H})$ position (the bottom of the half-circle).

grains, the additional spot $I(\boldsymbol{q} \perp \boldsymbol{H})$ in the diffraction pattern may be explained. Nevertheless, those simple (single-q) helix structures can hardly be reconciled with the emergence of the very large topological Hall effect as observed.

Hereafter, as the most plausible scenario, we adopt the standpoint that the skyrmion lattice is formed in MnGe. To identify the genuine magnetic contributions with $I(\boldsymbol{q} \parallel \boldsymbol{H})$ and $I(\boldsymbol{q} \perp \boldsymbol{H})$ or to eliminate the apparent variation of the scattering intensity by rotation of the grains, it is useful to discuss the H dependence of the intensity in a decreasing field, since we can reasonably assume that the grains remain locked in their positions once they have been aligned by the field. In fact, two independent field-decreasing scans show little difference [open and closed data points in Figs. 4(a) and 4(b)]. The neutron scattering cross section is proportional to $|\hat{\boldsymbol{q}} \times [\boldsymbol{M}(\boldsymbol{q}) \times \hat{\boldsymbol{q}}]|^2$ [$\boldsymbol{M}(\boldsymbol{q})$ being the Fourier transform of the magnetization], and hence the scattering intensity coming from the conical magnetic structure is proportional to the squared magnetization component perpendicular to the scattering vector, $M_\perp^2 = M_s^2 - M^2$. M_s stands for the nearly saturated magnetization, e.g., at 14 T, and M is the magnetization component parallel to the field. The H dependence of $I(\boldsymbol{q} \parallel \boldsymbol{H})$ is proportional to $M_s^2 - M^2$. On the other hand, $I(\boldsymbol{q} \perp \boldsymbol{H})$ only rises below approximately 4 T, which can clearly be seen in the development of the peak intensity at $\theta = 0$ in the angular dependence of the scattering intensity [Fig. 4(c)]. (Here, θ is defined as the angle of the q point in the q circle measured from the bottom $q \perp H$ point.) Disarray of the skyrmion lattice appears to occur at high fields, which may explain the decrease of $I(\boldsymbol{q} \perp \boldsymbol{H})$ above 4 T; this is reminiscent of the transformation into a heavily distorted skyrmion lattice or sparsely populated skyrmions as observed in an $Fe_{0.5}Co_{0.5}Si$ thin plate[10] and has been explained theoretically.[41]

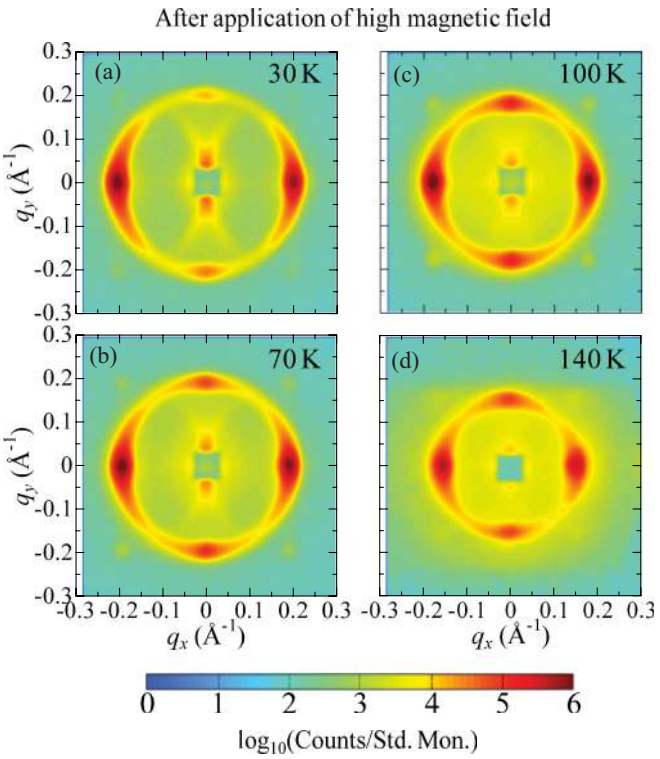

FIG. 5. (Color online) SANS patterns under zero magnetic field after an application of high magnetic field exceeding critical magnetic field at each temperature; 9.9 T for 30, 70, and 100 K and 5.0 T for 140 K. [See also Fig. 1(b).]

We have also examined the temperature range where $I(\boldsymbol{q} \perp \boldsymbol{H})$ appears, i.e., the possible skyrmion-lattice forms (Fig. 5). To exclude the possibility of a multidomain state of single-q helical structure, SANS patterns were taken at zero magnetic field after aligning the modulation vector by applying a high magnetic field above H_c at each temperature ($\mu_0 H =$ 9.9 T for 30, 70, and 100 K and $\mu_0 H = 5.0$ T for 140 K). There still exists $I(\boldsymbol{q} \perp \boldsymbol{H})$ at all the measured temperatures.[18,42] Thus, the skyrmion state is stable in a wide temperature range, perhaps over the whole temperature region below T_N (= 170 K).

B. Fitting of topological Hall resistivity

The quantum phase factor, the so-called Berry phase, can be multiplied with the wave function by the adiabatic change in the parameter on which the Hamiltonian depends. Conduction electrons in a non-coplanar spin structure can acquire the Berry phase Φ related to the spacial variation of the spin direction, and thus feel the gauge flux $\frac{\phi_0}{2\pi}\Phi$ in analogy with the Aharonov-Bohm phase. ($\phi_0 = h/e$.) The value of the Berry phase is equal to half of the solid angle subtended by the spins in the spherical surface of the spin space. In a skyrmion magnetic structure, the Berry phase collected by the conduction electrons is

$$\Phi = 2\pi \int d\boldsymbol{r}\, \boldsymbol{\Phi}^z = \frac{1}{2} \int d\boldsymbol{r}\, \hat{\boldsymbol{n}} \cdot \left(\frac{\partial \hat{\boldsymbol{n}}}{\partial x} \times \frac{\partial \hat{\boldsymbol{n}}}{\partial y} \right),$$

which can result in the topological Hall effect; the topological Hall resistivity ρ_{yx}^T is in proportion to Φ. Here $\boldsymbol{\Phi}^z$ is the skyrmion density, $\hat{\boldsymbol{n}} = \boldsymbol{M}(\boldsymbol{r})/|\boldsymbol{M}(\boldsymbol{r})|$, and the integration extends over one magnetic unit cell.

The H dependence of the topological Hall effect has been theoretically discussed for different forms of skyrmion lattices.[29–31] The profiles are different from each other, being sensitive to the lattice forms. Here, to estimate ρ_{yx}^T, we follow the method by Binz and Vishwanath[30] and discuss which type of lattice, square or SC, is more plausible for the case of MnGe. Assuming that the conduction electrons cannot couple to a part with smaller magnetization than some cutoff,[30] the collected Berry phase is modified as $\Phi = 2\pi \int d\boldsymbol{r}\, \Theta[|\boldsymbol{M}(\boldsymbol{r})| - M_c]\boldsymbol{\Phi}^z$, where Θ is the Heaviside step function and M_c is a cutoff magnetization.

The position dependence of the magnetization $\boldsymbol{M}(\boldsymbol{r})$ in the skyrmion lattice is described by a superposition of helices with identical handedness.[43] The handedness is determined by the sign of the DM interaction. The square and SC skyrmion lattices are superpositions of two and three orthogonal helical structures, respectively,

$$\begin{aligned} \boldsymbol{M}^{\mathrm{sq}}(\boldsymbol{r}) &= (0, \sin x, \cos x) + (-\sin y, 0, \cos y) + (0,0,m) \\ &= (-\sin y, \sin x, \cos x + \cos y + m) \end{aligned}$$

and

$$\begin{aligned} \boldsymbol{M}^{\mathrm{SC}}(\boldsymbol{r}) &= (0, \cos x, -\sin x) + (-\sin y, 0, \cos y) \\ &\quad + (\cos z, -\sin z, 0) + (0,0,m) \\ &= (-\sin y + \cos z, -\sin z + \cos x, \\ &\quad -\sin x + \cos y + m). \end{aligned}$$

Here, m is the induced magnetization, which should be almost linearly proportional to the applied field as observed.[18] The square and SC skyrmion lattices are illustrated in Figs. 6(a) and 6(b), respectively, where m was set to $m = 0$. Arrays of vortices pointing up ($M_z > 0$; red) and down ($M_z < 0$; blue) are arranged in an alternate order for these skyrmion lattices. We can see nodes with zero M, in the vicinity of which we neglect the collection of the Berry phase. Note that the choice of chirality of the skyrmion lattice, or equivalently the swirling direction in a skyrmion, changes neither the value of the Berry phase nor the topological Hall effect; here we take the superpositions of left-handed spirals.

The calculated results of the Berry phase with different cutoffs are shown in Figs. 6(d) and 6(e) as a function of magnetic field in comparison with the observed topological Hall resistivity at 30 K in MnGe.[18] The negative maximal value of the Berry phase and the critical field in the calculations are fitted with the experimental negative peak value of ρ_{yx}^T and H_c, respectively. Both the results of the square and SC lattices explain crudely the experimentally observed profile of ρ_{yx}^T: (i) $\rho_{yx}^T = 0$ at $H = 0$, (ii) a finite ρ_{yx}^T at $0 < H < H_c$, and (iii) $\rho_{yx}^T = 0$ at $H > H_c$. These behaviors can be qualitatively explained as follows: (i) positive (skyrmion) and negative (antiskyrmion) contributions cancel each other out at $H = 0$, (ii) finite m induced by a magnetic field breaks the balance of the contributions from skyrmions and antiskyrmions, yielding nonzero net spin chirality, (iii) a fully spin polarized state gives no Berry phase factor. Among them, the striking agreement with the experimental data in the SC lattice model with the cutoff of $M_c = 1/6$ is noteworthy, while

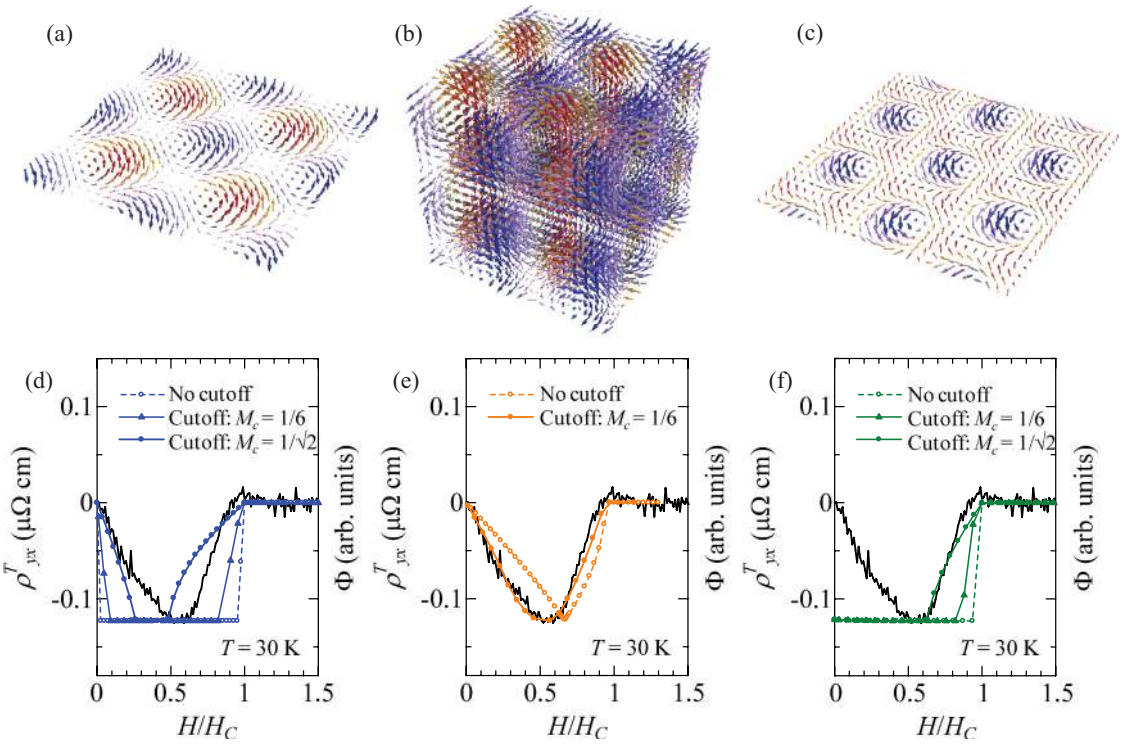

FIG. 6. (Color online) Schematic illustrations of (a) a square, (b) a simple-cubic, and (c) a triangular skyrmion lattice. The color and the hue of the arrows represent the z component of the magnetic moments; red (blue) arrows indicate up (down) magnetic moments. Comparison between the experimental results of topological Hall resistivity[18] (black solid lines) and the calculated ones with varying cutoff magnetization (M_c) in (d) a square, (e) a simple-cubic, and (f) a triangular skyrmion lattice.

the square lattice model cannot give a good fit with any arbitrary cutoff value. For comparison, we show in Fig. 6(f) the calculations of the Berry phase in the hitherto-known skyrmion lattice, i.e., the triangular lattice of antiskyrmions illustrated in Fig. 6(c). Because the triangular lattice is composed entirely of antiskyrmions producing a negative fictitious field, a finite topological Hall effect would be observed even at zero magnetic field,[31] which is discrepant with the observation. This also supports that a different form of skyrmion lattice, other than the triangular lattice, is realized in MnGe. However, the above calculations do not take the disarray of magnetic structure suggested by the SANS results into account, and hence the lattice form of the skyrmions in MnGe still remains inconclusive.

IV. CONCLUSIONS

We have observed the SANS peak whose q vector is perpendicular to magnetic field (H) in a wide T-H region including $H = 0$, which indicates the ground state with multiple-q vectors or the skyrmion-lattice state in $B20$-type MnGe. A small uniaxial distortion, which was observed experimentally by Makarova *et al.*,[39] may play a role in the stabilization of the skyrmion texture as theoretically predicted by Butenko *et al.*[44] The square and simple-cubic skyrmion lattices, whose magnetic modulation directions are described by the hybridization of two or three independent ⟨100⟩ crystal-axis directions, are plausible candidates. Although both lattice models can explain the overall H dependence of the topological Hall effect, the simple-cubic skyrmion lattice is more likely in light of the better fitting of ρ^T_{yx} as a function of H. In addition to the much smaller skyrmion-lattice constant (3–6 nm) in MnGe than other skyrmion systems (10–200 nm), the features revealed in this study are the tetragonal or cubic lattice form of the skyrmion crystal, not the hitherto-known hexagonal (triangular-lattice) form, and the ground-state ($H = 0$) skyrmion-lattice states possibly composed of alternating skyrmions and antiskyrmions.

The rapid reduction of $I(\boldsymbol{q} \perp \boldsymbol{H})$ in the high-field region remains elusive. A microscopic observation and/or a theoretical investigation on the magnetic structure under a magnetic field are left as challenges for future study as well as the full structural determination of the skyrmion lattice with use of a single crystal of MnGe.

ACKNOWLEDGMENTS

This work is based on experiments performed at the Swiss spallation neutron source SINQ, Paul Scherrer Institute, Villigen, Switzerland. The authors thank Y. Endoh, N. Nagaosa, D. Okuyama, and S. Seki for enlightening discussions. This work was supported by the Swiss National Science Foundation and its NCCR programme MaNEP, Grants-in-Aid for JSPS Fellows and Scientific Research (Grants No. 20340086, No. 22014003, No. 23684023, and No. 24224009) of Japan, and the FIRST Program by the Japan Society for the Promotion of Science (JSPS).

[1] I. Dzyaloshinskii, J. Phys. Chem. Solids **4**, 241 (1958).
[2] T. Moriya, Phys. Rev. **120**, 91 (1960).
[3] Y. Ishikawa and M. Arai, J. Phys. Soc. Jpn. **53**, 2726 (1984).
[4] C. Pfleiderer, D. Reznik, L. Pintschovius, H. V. Löhneysen, M. Garst, and A. Rosch, Nature (London) **427**, 227 (2004).
[5] A. Hamann, D. Lamago, Th. Wolf, H. V. Löhneysen, and D. Reznik, Phys. Rev. Lett. **107**, 037207 (2011).
[6] C. Pappas, E. Lelièvre-Berna, P. Bentley, P. Falus, P. Fouquet, and B. Farago, Phys. Rev. B **83**, 224405 (2011).
[7] M. Uchida, N. Nagaosa, J. P. He, Y. Kaneko, S. Iguchi, Y. Matsui, and Y. Tokura, Phys. Rev. B **77**, 184402 (2008).
[8] S. Mühlbauer, B. Binz, F. Jonietz, C. Pfleiderer, A. Rosch, A. Neubauer, R. Georgii, and P. Böni, Science **323**, 915 (2009).
[9] W. Münzer, A. Neubauer, T. Adams, S. Mühlbauer, C. Franz, F. Jonietz, R. Georgii, P. Böni, B. Pedersen, M. Schmidt, A. Rosch, and C. Pfleiderer, Phys. Rev. B **81**, 041203 (2010).
[10] X. Z. Yu, Y. Onose, N. Kanazawa, J. H. Park, J. H. Han, Y. Matsui, N. Nagaosa, and Y. Tokura, Nature (London) **465**, 901 (2010).
[11] X. Z. Yu, N. Kanazawa, Y. Onose, K. Kimoto, W. Z. Zhang, S. Ishiwata, Y. Matsui, and Y. Tokura, Nat. Mater. **10**, 106 (2010).
[12] H. Wilhelm, M. Baenitz, M. Schmidt, U. K. Rößler, A. A. Leonov, and A. N. Bogdanov, Phys. Rev. Lett. **107**, 127203 (2011).
[13] E. Moskvin, V. Dyadkin, H. Eckerlebe, M. Schmidt, H. Wilhelm, and S. V. Grigoriev, arXiv:1111.2200v1.
[14] C. Pfleiderer, T. Adams, A. Bauer, W. Biberacher, B. Binz, F. Birkelback, P. Böni, C. Franz, R. Georgii, M. Janoschek, A. Neubauer, B. Pedersen, and A. Rosch, J. Phys.: Condens. Matter **22**, 164207 (2010).
[15] N. Nagaosa and Y. Tokura, Phys. Scr., T **146**, 014020 (2012).
[16] A. Neubauer, C. Pfleiderer, B. Binz, A. Rosch, R. Ritz, P. G. Niklowitz, and P. Böni, Phys. Rev. Lett. **102**, 186602 (2009).
[17] Minhyea Lee, W. Kang, Y. Onose, Y. Tokura, and N. P. Ong, Phys. Rev. Lett. **102**, 186601 (2009).
[18] N. Kanazawa, Y. Onose, T. Arima, D. Okuyama, K. Ohoyama, S. Wakimoto, K. Kakurai, S. Ishiwata, and Y. Tokura, Phys. Rev. Lett. **106**, 156603 (2011).
[19] J. D. Zang, M. Mostovoy, J. H. Han, and N. Nagaosa, Phys. Rev. Lett. **107**, 136804 (2011).
[20] K. Everschor, M. Garst, R. A. Duine, and A. Rosch, Phys. Rev. B **84**, 064401 (2011).
[21] T. Schulz, R. Ritz, A. Bauer, M. Halder, M. Wagner, C. Franz, C. Pfleiderer, K. Everschor, M. Garst, and A. Rosch, Nat. Phys. **8**, 301 (2012).
[22] F. Jonietz, S. Mühlbauer, C. Pfleiderer, A. Neubauer, W. Münzer, A. Bauer, T. Adams, R. Georgii, P. Böni, R. A. Duine, K. Everschor, M. Garst, and A. Rosch, Science **330**, 1648 (2010).
[23] X. Z. Yu, N. Kanazawa, W. Z. Zhang, T. Nagai, T. Hara, K. Kimoto, Y. Matsui, Y. Onose, and Y. Tokura, Nature Commun. **3**, 988 (2012).
[24] S. Seki, X. Z. Yu, S. Ishiwata, and Y. Tokura, Science **336**, 198 (2012).
[25] A. Bogdanov and D. A. Yablonskii, Sov. Phys. JETP **68**, 101 (1989); A. Bogdanov and A. Hubert, J. Magn. Magn. Mater. **138**, 255 (1994).
[26] B. Binz, A. Vishwanath, and V. Aji, Phys. Rev. Lett. **96**, 207202 (2006).
[27] U. K. Rößler, A. N. Bogdanov, and C. Pfleiderer, Nature (London) **442**, 797 (2006).
[28] I. Fischer, N. Shah, and A. Rosch, Phys. Rev. B **77**, 024415 (2008).
[29] S. D. Yi, S. Onoda, N. Nagaosa, and J. H. Han, Phys. Rev. B **80**, 054416 (2009).
[30] B. Binz and A. Vishwanath, Physica B **403**, 1336 (2008).
[31] J. H. Park and J. H. Han, Phys. Rev. B **83**, 184406 (2011).
[32] T. Adams, S. Mühlbauer, C. Pfleiderer, F. Jonietz, A. Bauer, A. Neubauer, R. Georgii, P. Böni, U. Keiderling, K. Everschor, M. Garst, and A. Rosch, Phys. Rev. Lett. **107**, 217206 (2011).
[33] S. Kusaka, K. Yamamoto, T. Komatsubara, and Y. Ishikawa, Solid State Commun. **20**, 925 (1976).
[34] M. Date, K. Okuda, and K. Kadowaki, J. Phys. Soc. Jpn. **42**, 1555 (1977).
[35] K. Kadowaki, K. Okuda, and M. Date, J. Phys. Soc. Jpn. **51**, 2433 (1981).
[36] S. V. Grigoriev, S. V. Maleyev, A. I. Okorokov, Y. O. Chetverikov, and H. Eckerlebe, Phys. Rev. B **73**, 224440 (2006); S. V. Grigoriev, V. A. Dyadkin, D. Menzel, J. Schoenes, Y. O. Chetverikov, A. I. Okorokov, H. Eckerlebe, and S. V. Maleyev, *ibid.* **76**, 224424 (2007).
[37] M. Takeda, Y. Endoh, K. Kakurai, Y. Onose, J. Suzuki, and Y. Tokura, J. Phys. Soc. Jpn. **78**, 093704 (2009).
[38] C. Pfleiderer, Report No. FIRST-QS2C, FIRST-QS2C workshop on Emergent Phenomena of Correlated Materials, Okinawa, 2011 (unpublished).
[39] O. L. Makarova, A. V. Tsvyashchenko, G. Andre, F. Porcher, L. N. Fomicheva, N. Rey, and I. Mirebeau, Phys. Rev. B **85**, 205205 (2012).
[40] S. Okada, T. Shishido, M. Ogawa, F. Matsukawa, Y. Ishizawa, K. Nakajima, T. Fukuda, and T. Lundström, J. Cryst. Growth **229**, 532 (2001).
[41] U. K. Rößler, A. A. Leonov, and A. N. Bogdanov, J. Phys.: Conf. Ser. **303**, 012105 (2011).
[42] In the relatively high temperature region near below T_N, the topological Hall conductivity characteristic of the skyrmion state is decreased in magnitude due to the increased carrier scattering rate (or longitudinal resistivity),[18] and it can hardly be used to map the skyrmion-lattice state in the B-T phase diagram. In contrast, the present SANS study could clearly indicate the subsistence of the skyrmion-lattice state up to T_N.
[43] There are two main explanations about the driving force for the skyrmion-lattice formation: interaction between different q modes (Refs. 8 and 26) and nucleation of a localized entity (Refs. 27 and 41). However, the estimation of the topological Hall effect will be least affected by the origin of skyrmion-lattice formation because the magnetic structures described by the different models are similar to each other.
[44] A. B. Butenko, A. A. Leonov, U. K. Rößler, and A. N. Bogdanov, Phys. Rev. B **82**, 052403 (2010).